Dinuclear Copper(II) Cryptates of Macrocyclic Ligands: Synthesis, Crystal Structure, and Magnetic Properties. Mechanism of the Exchange Interaction through Bridging Azido Ligands

Jacques Comarmond,[†] Pierre Plumeré,[†] Jean-Marie Lehn,*[†] Yvette Agnus,[‡] Rémy Louis,[‡] Raymond Weiss,*[‡] Olivier Kahn,*[§] and Irène Morgenstern-Badarau[§]

Contribution from the Laboratoire de Chimie Organique Physique and the Laboratoire de Cristallochimie et de Chimie Structurale, Institut Le Bel, Université Louis Pasteur, 67000 Strasbourg, France, and the Laboratoire de Spectrochimie des Eléments de Transition, Université de Paris-Sud, 91405 Orsay, France. *Received August 19, 1981*

Abstract: The tetraazido dinuclear Cu(II) complexes **1** and **2** of the polyaza-polyoxa macrocyclic ligands **4**, [24]ane-N_2O_6, and **5**, [24]ane-N_6O_2, respectively, have been prepared, and their crystal structures have been determined. In both cases the two copper ions are contained inside the molecular cavity and are bound to the ONO and NNN chelating subunits situated at the two poles of the macrocycles **4** and **5**, respectively. **1** crystallizes in the monoclinic system, space group $P2_1/n$ (a = 17.780 (2) Å, b = 9.719 (1) Å, c = 17.361 (2) Å, β = 109.32 (5)°, Z = 4). In the $[N_3Cu(N_3)_2CuN_3 \subset$ **4**] unit the two Cu(II) centers are doubly bridged by two azide ions bound end-on, and each Cu(II) displays octahedral coordination with four equatorial nitrogens and two axial oxygens. The Cu-Cu distance is 3.162 Å, and the macrocycle is in a boat type conformation. **2** crystallizes in the monoclinic system, space group $C2/m$ (a = 9.533 (1) Å, b = 12.305 (1) Å, c = 11.913 (1) Å, β = 107.25 (4)°, Z = 2). In the $[N_3Cu(N_3)_2CuN_3 \subset$ **5**] unit, the two copper cations are pentacoordinate CuN_5 centers, with square-base pyramidal geometry, involving three ring nitrogens and two terminally bound azide ions; one of the azide ions is directed outside the ring and the other lies parallel to the intramolecular Cu-Cu axis, however without forming a symmetric head-to-tail bridge. The Cu-Cu distance is 5.973 Å, and the macrocycle is in a chair-type conformation. The temperature dependences of the magnetic susceptibilities for **1** and **2** were studied in the 3.8-300 K range. For **1**, the copper(II) ions are coupled in a ferromagnetic manner with the ground-spin triplet stabilized by 70 ± 20 cm^{-1} with regard to the singlet. In **2**, the copper(II) ions are noncoupled. The EPR spectra confirm the nature of the interaction in both **1** and **2**. The intramolecular ferromagnetic coupling observed in **1** is due to the nearly accidental orthogonality of the magnetic orbitals centered on the metal ions. In **2**, the absence of coupling arises from the unfavorable relative orientations of the magnetic orbitals. The study of the mechanism of the exchange through azido ligands has been extended to the related diazo-bridged dicopper(II) complex **3**, containing two SNS chelating subunits, which exhibits a diamagnetic behavior resulting from a very strong antiferromagnetic interaction; the origin of this interaction is attributed to the very similar energies and favorable relative orientation of the orbitals on the bridges and on the metallic centers.

Macropolycyclic structures containing two binding subunits form dinuclear cryptates by inclusion of two metal cations into the cavity defined by the molecular framework. The general ideas underlying the design of such systems have been presented, and a number of dimetallic cryptates of different structural types have been reported in recent years (see ref 1 and references therein). Various types of dinuclear complexes have been obtained with macrocycles containing two chelating subunits such as saturated macrocycles[1-4] or macrocyclic Schiff base and "compartmental" ligands.[5-9] In such complexes, the metal cations are bound to the chelating units and held by the macrocyclic framework at a distance and in a coordination arrangement that may allow further binding of a bridging species in a "cascade"-type complexation process.[1] Thus, dinuclear macrocyclic complexes containing imidazolato,[10-12] azido,[13,14] and hydroxo[13,15-18] bridges have been described. The interest of these types of complexes lies in the unusual physical properties that they may possess, in their significance as models of biological dimetallic sites,[19,20] and in their potential chemical reactivity as dinuclear catalysts.

We describe here the synthesis, the crystal structure, and the magnetic properties of the two related dinuclear Cu(II) complexes **1** and **2**, in which the cations are bound respectively to "ONO" and "NNN" chelating subunits contained in a 24-membered macrocycle and are bridged by two azide anions. We also present an interpretation of the magnetism of **1** and **2**, as well as of the related macrocyclic diazido-bridged dicopper(II) complex **3**, containing two "SNS" chelating units, which has been reported recently and shown to be *diamagnetic*.[14]

Synthesis of the Macrocyclic Ligands [24]ane-N_2O_6 (4) and

[†] Laboratoire de Chimie Organique Physique, Institut Le Bel, Université Louis Pasteur.

[‡] Laboratoire de Cristallochimie et de Chimie Structurale, Institut Le Bel, Université Louis Pasteur.

[§] Université de Paris-Sud.

(1) Lehn, J.-M. *Pure Appl. Chem.* **1980**, *52*, 2441-2459.
(2) Travis, K.; Busch, D. H. *J. Chem. Soc., Chem. Commun.* **1970**, 1041-1042.
(3) Mercer, M.; Truter, M. R. *J. Chem. Soc., Dalton Trans.* **1973**, 2469-2473.
(4) Newkome, G. R.; Kohli, D. K.; Fronczek, F. R.; Hales, B. J.; Case, E. E.; Chiari, G. *J. Am. Chem. Soc.* **1980**, *102*, 7608-7610.
(5) Groh, S. *Isr. J. Chem.* **1976**, *15*, 277-307. Casellato, U.; Vigato, P. A.; Fenton, D. E.; Vidali, M. *Chem. Soc. Rev.* **1979**, *8*, 199-220.
(6) Nelson, S. M. *Pure Appl. Chem.* **1980**, *52*, 2461-2476.
(7) Drew, M. G. B.; Rodgers, A.; McCann, M.; Nelson, S. M. *J. Chem. Soc., Chem. Commun.* **1978**, 415-416.
(8) Dancey, K. P.; Tasker, P. A.; Price, R.; Hatfield, W. E.; Brower, D. C. *J. Chem. Soc., Chem. Commun.* **1980**, 1248-1250.
(9) Gagné, R. R.; Henling, L. M.; Kistenmacher, T. J. *Inorg. Chem.* **1980**, *19*, 1226-1231.
(10) Coughlin, P. K.; Dewan, J. C.; Lippard, S. J.; Watanabe, E.-i.; Lehn, J.-M. *J. Am. Chem. Soc.* **1979**, *101*, 265-266.
(11) Drew, M. G. B.; Cairns, C.; Lavery, A.; Nelson, S. M. *J. Chem. Soc., Chem. Commun.* **1980**, 1122-1123.
(12) Coughlin, P. K.; Lippard, S. J.; Martin, A. E.; Bulkowski, J. E. *J. Am. Chem. Soc.* **1980**, *102*, 7616-7617.
(13) Drew, M. G. B.; McCann, M.; Nelson, S. M. *J. Chem. Soc., Chem. Commun.*, **1979**, 481-482.
(14) Agnus, Y.; Louis, R.; Weiss, R. *J. Am. Chem. Soc.* **1979**, *101*, 3381-3384.
(15) Motekaitis, R. J.; Martell, A. E.; Lehn, J.-M.; Watanabe, E.-i., unpublished results; see also ref 16.
(16) Lehn, J.-M.; Pine, S. H.; Watanabe, E.-i.; Willard, A. K. *J. Am. Chem. Soc.* **1977**, *99*, 6766-6768.
(17) Burk, P. L.; Osborn, J. A.; Youinou, M. T.; Agnus, Y.; Louis, R.; Weiss, R. *J. Am. Chem. Soc.* **1981**, *103*, 1273-1274.
(18) Coughlin, P. K.; Lippard, S. J. *J. Am. Chem. Soc.* **1981**, *103*, 3328-3329.
(19) Fee, J. A. *Struct. Bonding (Berlin)* **1975**, *23*, 1-60. Malkin, R.; Malmström, B. G. *Adv. Enzymol.* **1970**, *33*, 177-244.

0002-7863/82/1504-6330$01.25/0

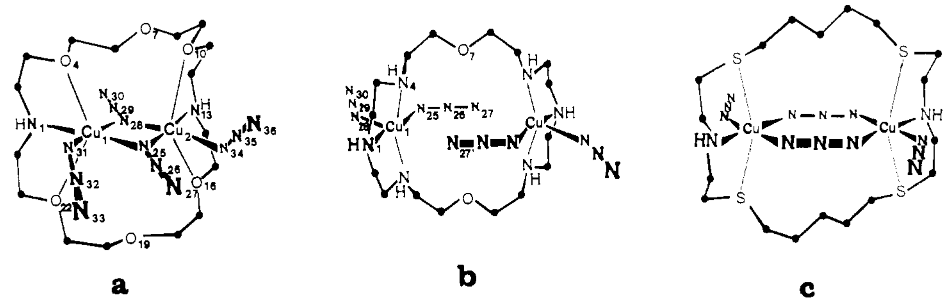

Figure 1. Molecular structure of **1–3** and the atom labeling: (a) for the Cu(II) complex of [24]ane-N_2O_6, $Cu_2(N_3)_4(C_{16}H_{34}N_2O_6)(H_2O)$ (**1**·H_2O); (b) for the bis Cu(II) complex of [24]ane-N_6O_2, $[Cu(N_3)_2]_2(C_{16}H_{38}N_6O_2)$ (**2**). The molecule is located on a symmetry center and presents $2/m$ (C_{2h}) crystallographic symmetry. The atom labeling used in the crystal structure data for complex **2** is different from the conventional labeling used for compound designation in the Experimental Section. (c) Structure of the Cu(II) complex of [24]ane-N_2S_4, $Cu_2(N_3)_4(C_{18}H_{38}N_2S_4)$ (**3**).

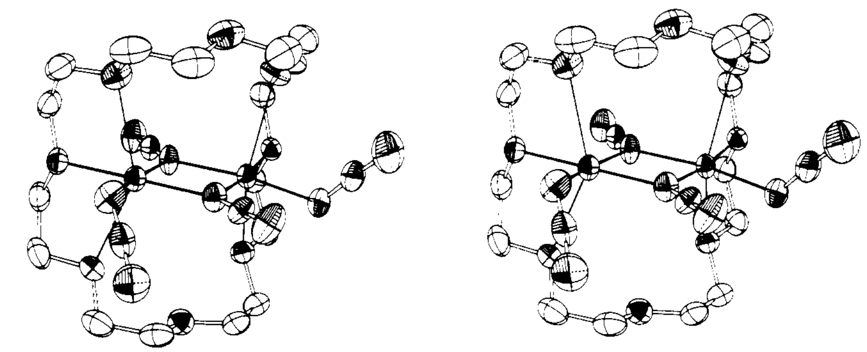

Figure 2. View of the complex molecule $Cu_2(N_3)_4$ $(C_{16}H_{34}N_2O_6)$ (**1**).

[24]ane-N_6O_2 (5) and of Their Dicopper(II) Complexes 1 and 2. The synthesis of the macrocycle **4** has been described earlier.[21]

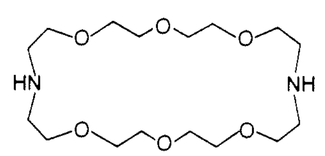

4

This 24-membered saturated ring, which contains two nitrogens and six oxygen atoms separated by ethylene units, may be designated by [24]ane-N_2O_6.

The bis(diethylenetriamine)macrocycle **5** has been prepared

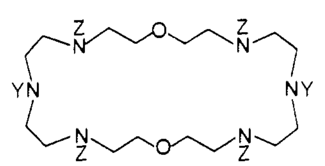

5, Y = Z = H
6a, Y = H; Z = tosyl
6b, Y = Z = tosyl

by two routes. Detosylation with HBr in acetic acid of the tetratosyl derivatives **6a**, obtained in the course of the synthesis of the dinucleating bis(2,2′,2″-triaminotriethylamine) [bis(tren)] macrobicycle,[16] gives **5** in about 75% yield.[22] However, for the purpose of the present work, where selective protection of four amino groups is not required, a more direct synthesis of **5** has been developed. Treatment of bis[2-(tosylamino)ethyl]tosylamine, $TsN(CH_2CH_2NHTs)_2$ (**7**), with 2-(2-chloroethoxy)ethanol, $ClCH_2CH_2OCH_2CH_2OH$, in presence of potassium carbonate affords the diol $TsN(CH_2CH_2NT_5CH_2CH_2OCH_2CH_2OH)_2$ (**8**). Reaction of its ditosylate $TsN(CH_2CH_2NTsCH_2CH_2OCH_2CH_2OTs)_2$ (**9**) with the disodium salt of **7** in dimethylformamide, following the method of Richman and Atkins,[23] gives a mixture of the desired (2 + 2) condensation product, the 24-membered macrocycle **6b**, and of the tritosylated 12-membered macrocycle [12]ane-N_3O. Detosylation of the mixture with HBr in acetic acid in presence of phenol yields a mixture from which the desired macrocycle [24]ane-N_6O_2 **5** may be isolated in 90% yield from **6b**.

The doubly bridged dinuclear Cu(II) complexes **1** and **2** are obtained by addition of sodium azide to a solution of the bis $Cu(ClO_4)_2$ complexes of **4** and **5** in methanol (see Experimental Section).

X-ray Crystal Structure of the Copper(II) Complex of [24]ane-N_2O_6, $Cu_2(N_3)_4(C_{16}H_{34}N_2O_6)(H_2O)$, 1·$H_2O$. The structure consists of discrete $Cu_2(N_3)_4(C_{16}H_{34}N_2O_6)$ molecules, resulting from the binding of a $Cu_2(N_3)_4$ unit into the macrocyclic ligand **4**, and water molecules. The atom labeling is given in Figure 1a. The structure of the complex molecule is shown in Figure 2. A stereoscopic view of the packing in the unit cell is shown in Figure 12.[48] Although the complex does not present any genuine symmetry element, a survey of all bond distance and bond angle values shows that it has a symmetry close to C_2, the C_2 axis going through the two axide ions N(25)–N(26)–N(27) and N(28)–N(29)–N(30). The conformation of the macrocyclic ligand is of a "boat" shape (Figure 2).

The two Cu(II) ions are located inside the macrocyclic cavity of ligand **4**. They are bonded each to an ONO set of donor atoms of the two diethanolamine chelating units at the two poles of the macrocycle. They are furthermore symmetrically linked together by a terminal nitrogen atom of each of the two azido bridges to give a $Cu_2(N_3)_2$ four-membered ring. Each Cu(II) completes its coordination through bonding with two independent terminal azido ligands. The two chromophores are of the type CuN_4O_2. Compound **1** may be formulated as the dinuclear *inclusion* complex $[N_3Cu(N_3)_2CuN_3 \subset 4]$.

The coordination polyhedron of each copper(II) is a (4 + 2) N_4O_2 octahedron, elongated in the direction of the two oxygen

(20) Solomon, E. I. In "Copper Proteins, Metal Ions in Biology"; Spiro, T. G., Ed.; Wiley: New York. 1981; Vol. 3. pp 41–108.
(21) Dietrich, B.; Lehn, J.-M.; Sauvage, J.-P.; Blanzat, J. *Tetrahedron* **1973**, *29*, 1629–1645.
(22) Lehn, J.-M.; Watanabe, E.-i., unpublished results.
(23) Richman, J. E.; Atkins, T. J. *J. Am. Chem. Soc.* **1974**, *96*, 2268–2270.

Table I. Bond Distances and Angles in the $Cu_2(N_3)_4(C_{16}H_{34}N_2O_6)(H_2O)$ Complex ($1 \cdot H_2O$) (in Å and Deg) with Estimated Standard Deviations in Parentheses

Cu(1)-N(1)	2.033 (2)	Cu(2)-N(13)	2.016 (3)
Cu(1)-N(25)	1.990 (2)	Cu(2)-N(25)	1.983 (2)
Cu(1)-N(28)	2.043 (2)	Cu(2)-N(28)	2.035 (2)
Cu(1)-N(31)	1.964 (2)	Cu(2)-N(34)	1.970 (2)
Cu(1)-O(4)	2.607 (3)	Cu(2)-O(10)	2.705 (3)
Cu(1)-O(22)	2.610 (3)	Cu(2)-O(16)	2.560 (3)
Cu(1)···Cu(2)	3.162 (0)	Cu(1)-N(25)-Cu(2)	105.46 (9)
N(25)···N(28)	2.490 (3)	Cu(1)-N(28)-Cu(2)	101.65 (8)
N(1)-Cu(1)-N(25)	173.07 (8)	N(13)-Cu(2)-N(25)	172.7 (1)
N(1)-Cu(1)-N(28)	97.36 (8)	N(13)-Cu(2)-N(28)	98.28 (9)
N(1)-Cu(1)-N(31)	90.68 (9)	N(13)-Cu(2)-N(34)	90.91 (9)
N(1)-Cu(1)-O(4)	73.05 (9)	N(13)-Cu(2)-O(10)	72.2 (1)
N(1)-Cu(1)-O(22)	73.29 (9)	N(13)-Cu(2)-O(16)	75.2 (1)
N(25)-Cu(1)-N(28)	76.24 (8)	N(25)-Cu(2)-N(28)	76.60 (8)
N(25)-Cu(1)-N(31)	95.87 (9)	N(25)-Cu(2)-N(34)	94.61 (9)
N(25)-Cu(1)-O(4)	109.84 (9)	N(25)-Cu(2)-O(10)	102.81 (9)
N(25)-Cu(1)-O(22)	104.3 (1)	N(25)-Cu(2)-O(16)	109.8 (1)
N(28)-Cu(1)-N(31)	171.38 (9)	N(28)-Cu(2)-N(34)	169.84 (9)
N(28)-Cu(1)-O(4)	95.36 (9)	N(28)-Cu(2)-O(10)	94.3 (1)
N(28)-Cu(1)-O(22)	95.3 (1)	N(28)-Cu(2)-O(16)	93.0 (1)
N(31)-Cu(1)-O(4)	83.9 (1)	N(34)-Cu(2)-O(10)	92.5 (1)
N(31)-Cu(1)-O(22)	89.9 (1)	N(34)-Cu(2)-O(16)	85.1 (1)
O(4)-Cu(1)-O(22)	145.6 (1)	O(10)-Cu(2)-O(16)	147.3 (1)
N(25)-N(26)	1.215 (3)	N(31)-N(32)	1.187 (3)
N(26)-N(27)	1.130 (3)	N(32)-N(33)	1.151 (3)
N(28)-N(29)	1.206 (3)	N(34)-N(35)	1.174 (3)
N(29)-N(30)	1.149 (3)	N(35)-N(36)	1.135 (4)
N(1)-C(2)	1.475 (4)	N(13)-C(14)	1.485 (4)
C(2)-C(3)	1.496 (3)	C(14)-C(15)	1.480 (4)
C(3)-O(4)	1.420 (3)	C(15)-O(16)	1.416 (5)
O(4)-C(5)	1.430 (4)	O(16)-C(17)	1.427 (4)
C(5)-C(6)	1.484 (4)	C(17)-C(18)	1.503 (3)
C(6)-O(7)	1.397 (3)	C(18)-O(19)	1.411 (4)
O(7)-C(8)	1.419 (2)	O(19)-C(20)	1.410 (4)
C(8)-C(9)	1.474 (3)	C(20)-C(21)	1.484 (3)
C(9)-O(10)	1.431 (4)	C(21)-O(22)	1.407 (4)
O(10)-C(11)	1.416 (4)	O(22)-C(23)	1.422 (4)
C(11)-C(12)	1.501 (3)	C(23)-C(24)	1.487 (4)
C(12)-N(13)	1.475 (3)	C(24)-N(1)	1.467 (3)
N(1)···N(28)	3.062 (2)	N(13)···N(28)	3.064 (3)
N(1)···N(31)	2.844 (3)	N(13)···N(34)	2.841 (3)
N(25)···N(31)	2.936 (3)	N(25)···N(34)	2.905 (3)

Cu(1)-N(25)-N(26)	128.7 (1)	Cu(2)-N(25)-N(26)	124.8 (1)
Cu(1)-N(28)-N(29)	131.7 (1)	Cu(2)-N(28)-N(29)	126.3 (1)
Cu(1)-N(31)-N(32)	126.0 (1)	Cu(2)-N(34)-N(35)	122.8 (2)
C(24)-N(1)-C(2)	112.6 (2)	C(12)-N(13)-C(14)	113.3 (2)
N(1)-C(2)-C(3)	110.2 (2)	N(13)-C(14)-C(15)	110.8 (2)
C(2)-C(3)-O(4)	108.2 (2)	C(14)-C(15)-O(16)	108.6 (2)
C(3)-O(4)-C(5)	112.9 (2)	C(15)-O(16)-C(17)	111.7 (2)
O(4)-C(5)-C(6)	108.3 (2)	O(16)-C(17)-C(18)	109.0 (2)
C(5)-C(6)-O(7)	109.9 (2)	C(17)-C(18)-O(19)	109.5 (2)
C(6)-O(7)-C(8)	114.5 (2)	C(18)-O(19)-C(20)	112.0 (2)
O(7)-C(8)-C(9)	109.3 (2)	O(19)-C(20)-C(21)	108.2 (2)
C(8)-C(9)-O(10)	108.4 (2)	C(20)-C(21)-O(22)	108.0 (2)
C(9)-O(10)-C(11)	111.1 (2)	C(21)-O(22)-C(23)	113.4 (2)
O(10)-C(11)-C(12)	108.5 (2)	O(22)-C(23)-C(24)	108.2 (2)
C(11)-C(12)-N(13)	111.6 (2)	C(23)-C(24)-N(1)	110.4 (2)

Dihedral Angles

N(1)-C(2)-C(3)-O(4)	59.6
C(2)-C(3)-O(4)-C(5)	−165.6
C(3)-O(4)-C(5)-C(6)	178.9
O(4)-C(5)-C(6)-O(7)	65.3
C(5)-C(6)-O(7)-C(8)	−167.1
C(6)-O(7)-C(8)-C(9)	158.9
O(7)-C(8)-C(9)-O(10)	−69.4
C(8)-C(9)-O(10)-C(11)	179.9
C(9)-O(10)-C(11)-C(12)	−179.3
O(10)-C(11)-C(12)-N(13)	−59.8
C(11)-C(12)-N(13)-C(14)	−166.6
C(12)-N(13)-C(14)-C(15)	175.1
N(13)-C(14)-C(15)-O(16)	61.4
C(14)-C(15)-O(16)-C(17)	−176.2
C(15)-O(16)-C(17)-C(18)	169.1
O(16)-C(17)-C(18)-O(19)	64.8
C(17)-C(18)-O(19)-C(20)	−174.0
C(18)-O(19)-C(20)-C(21)	170.2
O(19)-C(20)-C(21)-O(22)	−60.1
C(20)-C(21)-O(22)-C(23)	175.9
C(21)-O(22)-C(23)-C(24)	−178.8
O(22)-C(23)-C(24)-N(1)	−61.1
C(23)-C(24)-N(1)-C(2)	−169.5
C(24)-N(1)-C(2)-C(3)	170.5

atoms. The four nitrogen atoms are in equatorial positions and the two oxygen atoms in axial positions. The two octahedra share the edge N(25)···N(28). The main feature of structure **1** is the four-membered ring $Cu_2(N_3)_2$, which is symmetric and planar. This di-μ (end-on) azido bonding mode is also present in copper(II) azide, $Cu(N_3)_2$, which has a structure of infinite chains of planar $Cu(N_3)_2$ units,[24] and in $[Pd_2(N_3)_6][AsPh_4]_2$[25] and $(SbN_3Cl_4)_2$.[26,27] In **1** the Cu(1)···Cu(2)[28,29] and N(25)···N(28) distances are respectively 3.162 (1) and 2.490 (3) Å. Table I gives all bond distances and bond angles around the two copper ions. The four Cu–N bound distances range from 1.964 (2) to 2.043 (2) Å and the long Cu···O bond distances from 2.560 (3) to 2.705 (3) Å. The N–N bond distances in the azide ligands of **1** are different. The N_α–N_β distance (between 1.174 (3) and 1.215 (3) Å) is

Table II. Intermolecular Hydrogen Bonds and van der Waals Contacts Shorter than 3.50 Å in the Crystal Structure of $1 \cdot H_2O$ (Conventional ORTEP Notation)

N(27)···C(17)	|66502|	3.356			
N(27)···C(15)	|54501|	3.374			
N(27)···C(14)	|54501|	3.457			
N(30)···C(23)	|55504|	3.446			
N(31)···C(24)	|54504|	3.494			
N(32)···C(24)	|54504|	3.385			
N(33)···C(15)	|54501|	3.457			
N(36)···N(13)	|64504|	3.003	N(36)···H(13)	|64504|	2.347
N(36)···C(12)	|64504|	3.181	N(36)···H(12′)	|64504|	2.735
N(36)···C(14)	|64504|	3.255	N(36)···H(14′)	|64504|	2.734
O(7)···C(2)	|66602|	3.435			
O(19)···C(11)	|46403|	3.428			
O(0)···N(1)	|55504|	3.136	O(0)···H(1)	|55504|	2.473
O(0)···O(19)	|55501|	3.021			
O(0)···O(22)	|55501|	3.040			
O(0)···N(33)	|56501|	3.234			
O(0)···C(24)	|55504|	3.291	O(0)···H(24′)	|55504|	2.786
O(0)···O(16)	|55501|	3.356			
O(0)···C(2)	|55504|	3.376	O(0)···H(2′)	|55504|	2.876
O(0)···C(23)	|55501|	3.399			
O(0)···N(29)	|55501|	3.459			

(24) Söderquist, R. *Acta Crystallogr., Sect. B* **1968**, *B24*, 450–455. Agrell, I.; Lamnevik, S. *Acta Chem. Scand.* **1968**, *22*, 2038–2040. Agrell, I. *Ibid.* **1967** *21*, 2647–2658.

(25) Fehlhammer, W. P.; Dahl, L. F. *J. Am. Chem. Soc.* **1972**, *94*, 3377–3382.

(26) Müller, U. *Z. Anorg. Allg. Chem.* **1972**, *388*, 207.

(27) Agrell, I. *Acta Chem. Scand.* **1966**, *20*, 1281–1296; **1969**, *23*, 1667–1678.

(28) In a paramagnetic $[Cu^{II}_2(L)](ClO_4)_3$ compound containing a 28-membered macrocyclic ligand (L), the Cu–Cu bond distance is 2.445 (4) Å: Dancey, K. P.; Tasker, P. A.; Price, R.; Hatfield, W. E.; Brower, D. C. *J. Chem. Soc., Chem. Commun.* **1980**, 1248–1250. In $Cu_2(OH)_2$ units with two hydroxo bridges, the Cu···Cu separation is in the range 2.78–3.00 Å: Lewis, D. L.; McGregor, K. T.; Hatfield, W. E.; Hodgson, D. J. *Inorg. Chem.* **1974**, *13*, 1013–1019. In $Cu_2(CH_3COO)_4(H_2O)_2$ the Cu···Cu distance is 2.544 Å: Doedens, R. J. *Prog. Inorg. Chem.* **1976**, *21*, 209.

(29) In $[(CO)_3Mn(N_3)_3Mn(CO)_3](NEt_4)$ the two Mn cations are triply bridged by the three azide ligands through one terminal nitrogen atom in a tri-μ_3-(1.1.1)-azido (end-on) manner; the Mn···Mn distance is only 2.893 Å: Mason, R.; Rusholme, G. A.; Beik, W.; Englemann, H.; Joos, K.; Lindenberg, B.; Smedal, H. S. *J. Chem. Soc., Chem. Commun.* **1971**, 496–497.

(30) Supplementary material.

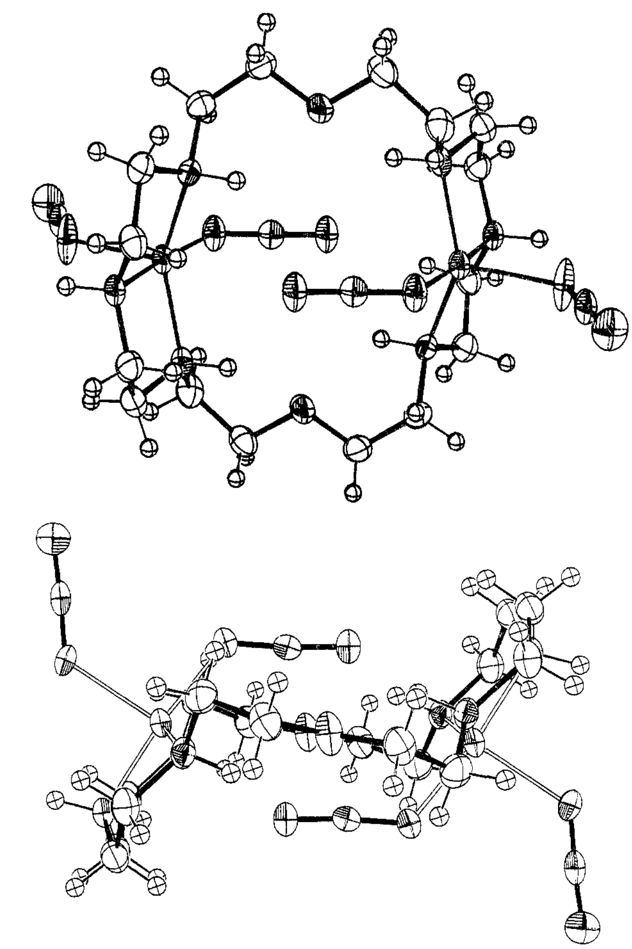

Figure 3. View of the complex molecule $(Cu(N_3)_2)_2(C_{16}H_{38}N_6O_2)$ (**2**) in two different orientations. The molecule presents $2/m$ (C_{2h}) crystallographic symmetry.

significantly greater than N_β–N_γ (between 1.130 (3) and 1.206 (3) Å). The Cu–N_α–N_β bond angles range from 122.8 (2) to 131.7 (1)° (see Table I).

The bond distances, bond angles, and dihedral angles other than those around the Cu(II) centers are given in Table I.

In the crystal, the molecules are linked by the two hydrogen bonds N(36)···N(13) and O(0)···N(1) and show van der Waals contacts. All these distances shorter than 3.50 Å are given in Table II.

X-ray Crystal Structure of the Copper(II) Complex of [24]-ane-N_6O_2 (2). The crystal structure of **2** consists of the packing of discrete molecules $[Cu(N_3)_2]_2(C_{16}H_{38}N_6O_2)$ resulting from the binding of two $Cu(N_3)_2$ units into the macrocyclic ligand **5**. The asymmetric unit and atom labeling scheme are given in Figure 1b. A view of the molecular structure is given in Figure 3. A spectroscopic view of the packing in the unit cell is shown in Figure 13.[48] The molecule is located on a symmetry center and presents $2/m$ (C_{2h}) crystallographic symmetry. The two Cu(II) ions, the four azide anions, and the two N(1) and N(13) nitrogen atoms of the macrocyclic ligand are situated in the symmetry plane; the two O(7) and O(19) oxygen atoms are located on the 2-fold axis.

The macrocyclic ligand in **2** adopts a "chair"-type conformation (Figure 3), which is apparently unstrained, as indicated by inspection of the bond distances, bond angles, and dihedral angles.

The two Cu(II) ions are located inside the macrocyclic ligand **5**, [24]ane-N_6O_2, linked each to a NNN ligand donor set of the two diethylenetriamine chelating sequences at the two poles of the macrocyclic cavity and to two nitrogen atoms of two end-on-bound azide ions. The two independent copper(II) centers are of the CuN_5 type. One azide ion, N(28)–N(29)–N(30), is directed outside the cavity of the macrocyclic ligand, and the other one, N(25)–N(26)–N(27), inside the cavity parallel to the intramolecular Cu···Cu axis. The molecular structure of this paramagnetic binuclear Cu(II) complex is similar to that of the diamagnetic complex **3**.[14] Compound **2** may be formulated as the dinuclear inclusion complex [N_3CuN_3, N_3CuN_3 $\subset$ **5**]. The crystal structure of an imidazolate-bridged bis Cu(II) complex of the same ligand, **5**, has been reported,[10] as well as another similar complex of the bis(diethylenetriamine) macrocycle in which CH_2 groups replace the O atoms of **5**.[12]

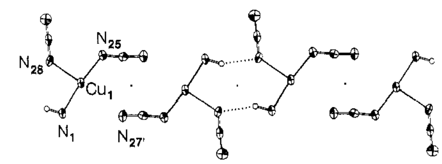

Figure 4. Hydrogen bonding scheme between two nearest complex molecules **2** along the *c* axis in the crystallographic symmetry plane; the macrocyclic ligand is omitted except for the two N(1) and N(13) nitrogen atoms. The Cu···Cu interatomic distances are alternatively 5.973 (1) Å (intramolecular) and 5.980 (1) Å (intermolecular). The same hydrogen bonding scheme is present in the diamagnetic compound **3** with Cu···Cu distances of 5.145 (1) Å (intramolecular) and 6.043 (1) Å (intermolecular); see ref 14.

Table III. Bond Distances and Angles in the $[Cu(N_3)_2]_2(C_{16}H_{38}N_6O_2)$ Complex (2) (in Å and Deg) with Estimated Standard Deviations in Parentheses

Cu···Cu	5.973 (1)		
Cu–N(1)	2.026 (3)	Cu–N(28)	2.181 (4)
Cu–N(4)	2.081 (2)	Cu···N(27′)	2.999 (4)
Cu–N(25)	1.963 (3)		
N(1)–Cu–N(4)	83.67 (7)	N(4)–Cu···N(27′)	71.71 (7)
N(1)–Cu–N(25)	174.1 (1)	N(4)–Cu–N(28)	107.86 (6)
N(1)–Cu···N(27′)	85.71 (7)	N(25)–Cu···N(27′)	88.35 (8)
N(1)–Cu–N(28)	90.1 (1)	N(25)–Cu–N(28)	95.8 (1)
N(4)–Cu–N(22)	141.99 (7)	N(28)–Cu···N(27′)	175.85 (8)
N(4)–Cu–N(25)	94.47 (7)		
N(1)–C(2)	1.476 (3)	N(4)–C(5)	1.486 (3)
C(2)–C(3)	1.506 (4)	C(5)–C(6)	1.499 (4)
C(3)–N(4)	1.483 (3)	C(6)–O(7)	1.421 (3)
N(25)–N(26)	1.187 (5)	N(28)–N(29)	1.183 (5)
N(26)–N(27)	1.159 (5)	N(29)–N(30)	1.155 (5)
N(1)···N(4)	2.740	O(7)···N(25)	3.985
N(1)···N(25)	3.984	O(7)···N(27′)	3.595
N(1)···N(27′)	3.491	N(25)···N(27′)	3.537
N(1)···N(28)	2.981	N(25)···N(28)	3.079
N(4)···O(7)	2.851	N(26)···N(26′)	3.431
N(4)···N(25)	2.970	N(26)···N(27′)	3.254
N(4)···N(27′)	3.067	N(27)···N(27′)	3.477
N(4)···N(28)	3.446		
N(25)–N(26)–N(27)	175.0 (4)	Cu–N(25)–N(26)	124.6 (3)
N(28)–N(29)–N(30)	177.3 (4)	Cu–N(28)–N(29)	128.0 (3)
C(24)–N(1)–C(2)	112.8 (2)	N(4)–C(5)–C(6)	112.8 (2)
N(1)–C(2)–C(3)	108.7 (2)	C(5)–C(6)–O(7)	107.2 (2)
C(2)–C(3)–N(4)	108.2 (2)	C(6)–O(7)–C(8)	112.4 (3)
C(3)–N(4)–C(5)	113.6 (2)		
Dihedral Angles			
C(24)–N(1)–C(2)–C(3)	−159.6	C(3)–N(4)–C(5)–C(6)	−90.2
N(1)–C(2)–C(3)–N(4)	52.6	N(4)–C(5)–C(6)–O(7)	−60.7
C(2)–C(3)–N(4)–C(5)	179.5	C(5)–C(6)–O(7)–C(8)	−170.2

The Cu–N bond distances and the N–Cu–N bond angles are given in Table III. All the other bond distances, bond angles, and dihedral angles are listed also in Table III. The intramolecular Cu···Cu distance in **2** is 5.973 (1) Å, whereas it is 5.145 (1) Å within the $Cu_2(N_3)_2$ ring of **3**.[14] Whereas in **3** the two azide ions form a symmetrical *double bridge* between the two Cu(II) cations, this is not the case in **2** where the Cu–N_γ distance (e.g., Cu···N(27′) = 2.999 (4) Å) is much longer than Cu–N_α (1.963 (3) Å, Table III) (Figures 1b and 4). In **3**, Cu–N_α and Cu–N_γ are 2.013 (3) and 1.994 (3) Å[14] (Figure 1c).

The symmetry of the coordination polyhedron of each copper ion is close to C_{4v}, derived from an octahedron elongated along

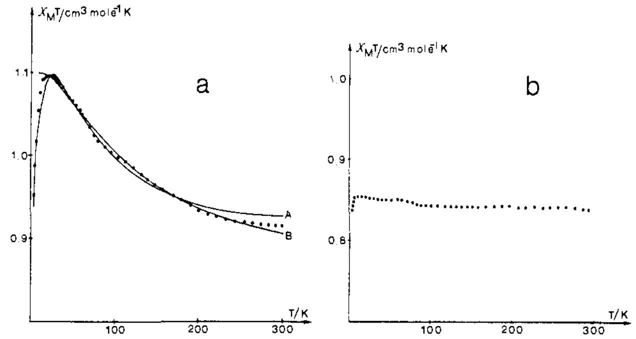

Figure 5. (a) Temperature dependence of $\chi_M T$ for complex **1**: experimental data (●) and calculated curves (—) (see text); (b) temperature dependence of $\chi_M T$ for complex **2**.

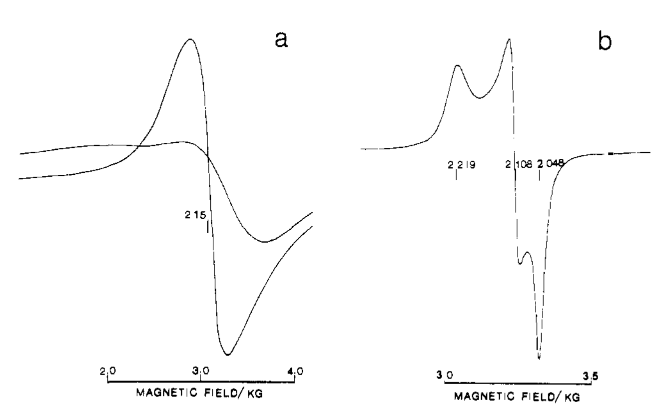

Figure 6. (a) Crystal EPR spectrum of compound **1** at 50 K for two orthogonal orientations of the magnetic field; (b) powder EPR spectrum of compound **2** in the region $M_s = 1$.

the N(28)···N(27′) axis situated in the symmetry plane. It is best described as a slightly distorted square-based pyramid[31] with the N(28) nitrogen atom on the apical position and the N(1), N(4), N(22), and N(25) nitrogen atoms defining the basal plane. The apical nitrogen is the terminal N(28) atom of the azido ligand located outside the cavity of the macrocycle, with a long Cu–N(28) bond distance of 2.181 (4) Å. The three independent Cu–N bond distances in the basal plane are 1.963 (3), 2.026 (3), and 2.081 (2) Å with two bond angles of 83.67 (7) and 94.47(7)°. The Cu atoms lie 0.37 Å above the mean basal plane. The two basal planes of the Cu ions are crystallographically parallel and 4.330 Å apart. In **3**, the coordination geometry of each copper ion is also an elongated octahedron with the S–Cu–S axis perpendicular to the symmetry plane.[14]

The two independent azide ions of **2** are essentially linear with N_α–N_β–N_γ bond angles of 175.0 (4) and 177.3 (4)°. The Cu–N_α–N_β bond angles are 124.6 (3) and 128.0 (3)°. The N_α–N_β and N_β–N_γ bond lengths are different in compound **2**, but they are the same in **3** and in other complexes incorporating a $M_2(N_3)_2$ ring.[14,32,33] In several nondimeric copper(II) azido complexes involving coordination of one end of the azide ion, small differences in the two azide bond lengths have been noted.[34–36] The two N–N distances in **2** are significantly different, with N_α–N_β 1.187 (5) and 1.183 (5) Å and N_β–N_γ 1.159 (5) and 1.155 (5) Å, the longer bond involving the nitrogen N_α attached to the metal.

In the crystal, the complex molecules are joined by hydrogen bonds forming chains along the *c* axis. All the Cu(II) ions are almost aligned along the direction of the *c* axis, and the Cu···Cu interatomic distances are alternatively 5.973 (1) Å (Cu···Cu intramolecular) and 5.980 (1) Å (Cu···Cu intermolecular). The hydrogen bonding scheme between two nearest molecules is pictured in Figure 4.

Magnetic and EPR Data. Results and Discussion

Results. The *magnetic behavior* of **1** is shown in Figure 5a in the form of the variation of $\chi_M T$ vs. T. $\chi_M T$ increases when cooling down and appears to reach a maximum equal to 1.10 cm³ mol⁻¹ K at about 30 K, to remain almost constant down to 18 K, and then to decrease slightly down to a value of 0.95 cm³ mol⁻¹ K at 4 K. This behavior is characteristic of a ferromagnetic coupling[37] between the copper(II) ions stabilizing the triplet state with regard to the singlet state. Two alternative strategies may be utilized to determine J, the singlet–triplet energy gap: (i) Since the decrease of $\chi_M T$ below 18 K suggest that a very weak antiferromagnetic intermolecular interaction superimposes itself on the intramolecular ferromagnetic coupling, one can account for this intermolecular effect with a θ Weiss correction. The theoretical expression for the magnetic susceptibility of the dimer is then

$$\chi_M = \frac{2N\beta^2 g^2}{k(T-\theta)}[3 + \exp(-J/kT)]^{-1} \qquad (1)$$

where the N, β, and k constants have their usual meaning. The values of the g, J, and θ parameters, determined by least-squares procedure, are $g = 2.16$, $J = 58$ cm⁻¹, and $\theta = -1.2$ K. The agreement factor defined by $\sum T^2(\chi_{obsd} - \chi_{calcd})^2/\sum T^2(\chi_{obsd})^2$ is equal to 3×10^{-4}. It must be noted here that a zero field splitting of the ground triplet state may also contribute to the magnetic behavior in the very low temperatures range. (*ii*) The plateau of the $\chi_M T$ vs. T plot between 30 and 18 K may be interpreted as a Curie law for a triplet state ($\chi_M T = 2N\beta^2 g^2/3k$), the singlet state being totally depopulated in this temperature range. The average value of the g factor is then 2.10. By keeping this g value and neglecting the experimental data below 18 K, the J value obtained by least-squares procedure from expression 1 with $\theta = 0$ is 83 cm⁻¹. The agreement factor is then again equal to 3×10^{-4}. The theoretical curves corresponding to the two approaches (noted A and B, respectively) are compared to the experimental data in Figure 5a. At first glance, the difference in the J values depending on the approach used to fit the experimental data may appear disappointing. It must be emphasized that in copper(II) dimers, the theoretical variation of the magnetic susceptibility is much more sensitive to small variations of J when the coupling is antiferromagnetic than when the coupling is ferromagnetic. The ratio $[\chi_M T(T \to \infty)]/[\chi_M T(T \to 0)]$ is infinitely large in the former case and equal to $^3/_4$ in the latter. By comparison of the effect of small changes in the J parameter with the experimental uncertainty, the uncertainty on each J determination is ±15 cm⁻¹. Thus, at best, we can assert that in **1**, J is in the range 50–90 cm⁻¹. This might seem a rather large uncertainty; however, we feel that the accuracy of the J values in case of ferromagnetic coupling has been generally overestimated.

The magnetic behavior of **2** is shown in Figure 5b, again in the form of the variation of $\chi_M T$ vs. T; $\chi_M T$ is nearly constant except below 8 K where it decreases slightly. This indicates that the two Cu(II) ions in the cryptate cavity are essentially noncoupled. Around 10 K, where the effect of the corrections of diamagnetism

(31) This geometry is similar to that observed in serveral complexes with N_3 diethylene-triamine (dien) nitrogens set in the basal planes; e.g., for 2-[Cu(dien)][Fe(CN)$_6$]$^+$ see: Morpurgo, G. O.; Mosini, V.; Porta, P.; Dessy, G.; Fares, V. *J. Chem. Soc., Dalton Trans.* **1981**, 111–117. Cu(dien)(NCS)$_2$: Cannas, M.; Carta, G.; Marongin, G. *Ibid.* **1974**, 553–555. [Cu$_2$(Me$_5$dien)$_2$(BiIm)](BPh$_4$)$_2$: Haddad, M. S.; Duesler, E. N.; Hendrickson, D. N. *Inorg. Chem.* **1979**, *18*, 141–148.

(32) See the di-μ-(1,3)-azido end-to-end ring in the dimeric complex [Cu$_2$(Me$_5$ dien)$_2$(N$_3$)$_2$](BPh$_4$)$_2$: Felthouse, T. R.; Hendrickson, D. N. *Inorg. Chem.* **1978**, *17*, 444–456. The data for this complex are d(Cu–Cu) = 5.2276 (7) Å and $J = -6.5$ cm⁻¹.

(33) The $M_2(N_3)_2$ ring is found in complexes with M = Cu(I), Ni(II): Cu$^I_2$(PPh$_3$)$_4$(N$_3$)$_2$: Ziolo, R. F.; Gaughan, A. P.; Dori, Z.; Pierpont, C. G.; Eisenberg, R. *J. Am. Chem. Soc.* **1970**, *92*, 738–739; *Inorg. Chem.* **1971**, *10*, 1289–1296. [Ni$_2$(tren)$_2$(N$_3$)$_2$](BPh$_4$)$_2$: Pierpont, C. G.; Hendrickson, D. N.; Duggan, D. M.; Wagner, F.; Barefield, E. K. *Ibid.* **1975**, *14*, 604–610. In the two cases, the $M_2(N_3)_2$ rings are not planar.

(34) Dori, Z.; Ziolo, R. F. *Chem. Rev.* **1973**, *73*, 247–254.

(35) Müller, U. *Struct. Bonding (Berlin)* **1973**, *14*, 141–172.

(36) Gaughan, A. P.; Ziolo, R. F.; Dori, Z. *Inorg. Chem.* **1971**, *10*, 2776–2781.

(37) Kahn, O.; Galy, J.; Tola, P.; Coudanne, M. *J. Am. Chem. Soc.* **1978**, *100*, 3931–3933.

and of TIP is minimized, $\chi_M T = 0.86$ cm^3 mol^{-1} K. For two noncoupled Cu(II) ions, this Curie constant corresponds to the average value of 2.13 for the g factor ($\chi_M T = N\beta^2 g^2/2k$).

The *crystal EPR spectra* of **1**·H_2O are shown in Figure 6a for two different orientations of the magnetic field. The main feature is an intense resonance, whose position varies very little with the orientations of the magnetic field. The temperature dependence of its intensity in the low-temperature range (4–50 K) confirms that the observed resonance occurs in the ground state. For some orientations of the magnetic field, a shift toward higher field and a clear decrease in the intensity of the main peak are observed at the same time that a bump appears at lower field. The very small anisotropy of the **g** tensor prevents any determination of the principal values. From the position of the intense peak, we determine a nearly isotropic g value of 2.15, very close to one of the values obtained from the magnetic data. We assigned the observed bump at lower field to the second allowed transition in the triplet state with a nearly axial zero field splitting tensor. The ill definition of the bump does not allow evaluation of the D parameter. Whatever the orientation of the magnetic field, no resonance is detected in the $\Delta M_s = 2$ region. This could be due to the very weak zero field splitting. Perhaps also, the $\Delta M_s = 2$ signal is hidden by the low-field side of the bump.

The *EPR spectrum* of **2** shown in Figure 6b is essentially unmodified between 4 K and room temperature. It is characteristic of a noncoupled copper(II) ion in a rhombic environment. The principal values of the **g** tensor are $g_1 = 2.219$, $g_2 = 2.108$, and $g_3 = 2.048$, with g_1 presumably along the apical direction Cu–N(28). The average g value is equal to 2.126, in agreement with the value determined from the magnetic data. In the $\Delta M_s = 2$ region, the EPR spectrum does not exhibit any signal.

Orbital Mechanism of the Interaction through μ-Azido Ligands. The discussion on the mechanism of the exchange interaction bears also on complex **3**[14] in addition to **1** and **2**. In spite of the large Cu···Cu separation (5.145 Å), **3** is diamagnetic, without EPR signal, in the whole temperature range 4.2–390 K. This means that the singlet–triplet energy gap J is too large in absolute value to be measured by the magnetic susceptibility technique. The two Cu(II) ions are therefore very strongly coupled in an antiferromagnetic manner.

The large spectrum of magnetic properties covered by **1–3** offers to us an unique opportunity to study thoroughly the mechanism of the interaction through bridging azido ligands. We note at the outset that, since the Cu(II) centers are not coupled in **2**, the couplings observed in **1** and **3** must be due to *intracavity* interactions and not to intermolecular interactions transmitted by the same intercomplex hydrogen bonding pattern (Figure 4) found in complexes **2** and **3**. Before discussing successively each of the compounds, we recall some essential results concerning the theory of the exchange interaction in copper(II) dimers, limited to complexes in which the ions are located in identical environments.

The interaction between two spin-doublets leads to two molecular levels characterized by $S = 0$ and $S = 1$ and separated by the energy J. J is negative when the singlet state is the lowest. When the interaction is weak enough in order for the two spin levels to be thermally populated at room temperature, J may be expressed as the sum of a negative antiferromagnetic contribution J_{AF} and of a positive ferromagnetic contribution J_F:[38,39]

$$J = J_{AF} + J_F$$

with

$$J_{AF} = -2\Delta S \qquad J_F = 2C \tag{2}$$

S is the overlap integral between the two magnetic orbitals ϕ_A and ϕ_B centered on the one and the other metallic ions; Δ is the energy gap between the two molecular orbitals noted γ and γ', constructed from ϕ_A and ϕ_B for the triplet state and C is the two-electron exchange integral $\langle \phi_A(1)\phi_B(2)|r_{12}^{-1}|\phi_A(2)\phi_B(1)\rangle$. The magnetic orbital ϕ_A (or ϕ_B) is defined as a singly occupied orbital centered on A (or B) and partially delocalized toward the ligands surrounding A (or B).

From a theoretical point of view, the simplest situation corresponds to the strict orthogonality of the magnetic orbitals[39] due to the molecular symmetry. S and J_{AF} are then identically zero and J equals J_F. The magnetic orbitals may also be accidentally or nearly accidentally degenerate (situation I). Contrary to the previous case, ϕ_A and ϕ_B are not out of symmetry. However, for very peculiar values of the structural parameters, S may be zero or very close to zero. This occurs when the positive zones of the overlap density compensate the negative zones. The distinction between strict orthogonality and accidental orthogonality is discussed in ref 39.

A different situation, noted II, is obtained when the relative orientations of the magnetic orbitals ϕ_A and ϕ_B are unfavorable to interaction. The overlap density defined $\rho(i) = \phi_A(i)\phi_B(i)$ is then negligible in any point of the space. Therefore, in **2**, S, C, and the two contributions J_{AF} and J_F are zero. Each chromophore formed by a Cu(II) ion surrounded by its nearest neighbors is isolated with regard to the other one in the dinuclear entity, and the magnetic and the EPR properties will be those of each chromophore.[40]

The most frequently encountered situation in Cu(II) dimers is that where the J_{AF} contribution predominates. When the antiferromagnetic interaction becomes strong enough in order for the spin triplet to be totally depopulated at room temperature (situation III), the pure Heitler–London wave functions are no longer appropriate to describe the low-lying states. In the borderline case of very strong interaction, the wave function constructed from the γ and γ' molecular orbitals may describe reasonably well the ground singlet state and the excited triplet state. These functions arise from the configurations γ^2 and $\gamma\gamma'$, respectively, and the stabilization of the singlet state with regard to the triplet becomes Δ instead of $2\Delta S$. Such a situation where the interaction is strong enough for the relations (**2**) to be no longer valid can occur when the unpaired electrons are very strongly delocalized toward the same bridging ligands. This requires that the highest occupied orbitals of the bridges and the singly occupied metal orbitals have very similar energies and a favorable relative orientation.

We now show how situation I applies itself to **1**, situation II to **2**, and situation III to **3**.

Compound 1. The coordination polyhedron relevant to the discussion of the magnetic properties of **1** is obvious in Figure 2. We idealized somewhat the actual structure by assuming a D_{2h} molecular symmetry, taking for the Cu–N–Cu bridging angles the average value of 103.6°. The metal orbitals involved in the exchange phenomenon are the d_{xy}'s pointing toward the terminal and bridging nitrogen atoms; they have the same b_1 site symmetry. Consequently we may assert that the observed ferromagnetic coupling does not result from a strict orthogonality of the magnetic orbitals. The question is why are the magnetic orbitals almost accidentally orthogonal.

As has been shown experimentally[41] and discussed theoretically,[39,42] the planar network **10** allows this situation of accidental orthogonality to occur. One can explain this behavior in two ways

(38) Kahn, O.; Briat, B.; Galy, J. *J. Chem. Soc., Dalton Trans.* **1977**, 1453–1457. Girerd, J. J.; Charlot, M. F.; Kahn, O. *Mol. Phys.* **1977**, *34*, 1063–1076.

(39) Kahn, O.; Charlot, M. F. *Nouv. J. Chim.* **1980**, *4*, 567–576. Kahn, O.; Galy, J.; Journaux, Y.; Jaud, J.; Morgenstern-Badarau, I. *J. Am. Chem. Soc.* **1982**, *104*, 2165–2176.

(40) A very peculiar and interesting situation, not encountered in this work, is where the two contributions J_{AF} and J_F compensate themselves exactly so that J is zero although the metallic ions interact. This situation cannot be distinguished from situation II by magnetic measurements. Indeed, two spin doublets of the same energy lead to the same Curie law as an accidentally degenerate spin singlet and spin triplet. However, EPR spectroscopy, which gives a doublet state in situation II and a triplet state in the present situation should allow one to make a distinction.

(41) Crawford, V. M.; Richardson, H. W.; Wasson, J. R.; Hodgson, D. J.; Hatfield, W. E. *Inorg. Chem.* **1976**, *15*, 2107–2110. Hodgson, D. J. *Ibid.* **1976**, *15*, 3174–3175.

(42) Hay, P. J.; Thibeault, J. C.; Hoffmann, R. *J. Am. Chem. Soc.* **1975**, *97*, 4884–4899.

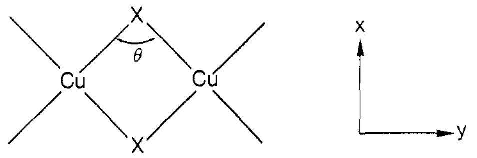

10

different in the formulation but equivalent as for the conclusions: (i) From the two magnetic orbitals of b_1 site symmetry, one can construct two molecular orbitals transforming as b_{1g} and b_{2u}. For a θ_0 value of the θ bridging angle, these molecular orbitals are accidentally degenerate and the energy gap Δ involved in **2** is zero. For $\theta < \theta_0$, b_{2u} is higher in energy than b_{1g}.[39,42] For $\theta > \theta_0$, the opposite situation holds. When the X bridges are very electronegative, the s valence orbitals of the bridges are too low in energy to interact with the d_{xy} metal orbitals and θ_0 is very close to 90°. When X is made less electronegative, the d_{xy}–s separation decreases; this interaction destabilizes b_{2u} with regard to b_{1g} and hence shifts θ_0 to larger θ. (ii) The overlap density $\rho(i) = \phi_A(i)\phi_B(i)$ between the magnetic orbitals exhibits around each of the bridges X two positive lobes along the y axis and two negative lobes along the x axis. For $\theta = \theta_0$, the positive lobes compensate the negative lobes, and the overlap integral is zero. For $\theta > \theta_0$ the overlap is negative, and for $\theta < \theta_0$ the overlap is positive. When the bridges are made less electronegative, the d_{xy}–s interaction increases the altitude of the positive lobes with regard to the depths of the negative lobes, and θ_0 is displaced to larger θ.[39]

For planar hydroxy-bridged copper(II) dimers, the orthogonality occurs for a θ value around 90°, so that for any $\theta < 97.5°$, the J_F contribution is predominant and the observed coupling is ferromagnetic.[41] On the contrary, for any $\theta > 97.5°$, J_{AF} is the dominant contribution; for $\theta = 103.6°$, a very strong antiferromagnetic coupling is expected, characterized, from Hatfield and Hodgson's correlation,[41] by $J \sim -450$ cm^{-1}. In **1** the bridging atoms are less electronegative, θ_0 is displaced toward larger θ, so that for $\theta = 103.6°$, J_F predominates. Figure 7 shows the variations of the energies of the b_{1g} and b_{2u} molecular orbitals against θ for the two model complexes **11** and **12** as obtained by extended

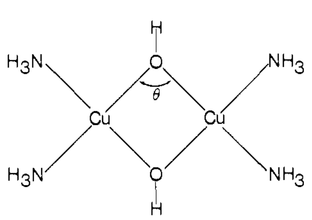

11

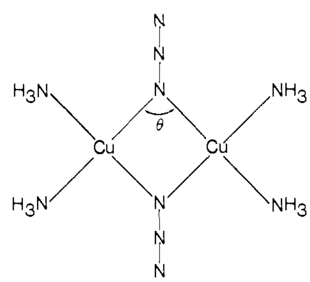

12

Hückel calculations.[43] The crossing point is calculated to be $\theta = 92°$ for **11** and $\theta = 103°$ for **12**. Moreover, for any θ value in the range 90–110°, Δ for **12** remains very weak. Figure 8 represents the b_{1g} and b_{2u} molecular orbitals in compound **1**. A weak ferromagnetic coupling has already been reported for Cu(acac)N_3 in which N_3 also bridges the two copper(II) ions in a end-on fashion.[44]

Compound 2. The environment of each Cu(II) ion is a CuN_5 square pyramid (obvious in Figures 3 and 4). Choosing the apical direction as the z axis and the basal plane as the xy plane, the magnetic orbital ϕ_A (or ϕ_B) has a metallic contribution of the form $ad_{xy} + bd_{z^2}$ with $a^2 \gg b^2$. The two magnetic orbitals are represented in Figure 9. Their relative orientations are particularly unfavorable for transmitting the electronic effects between two

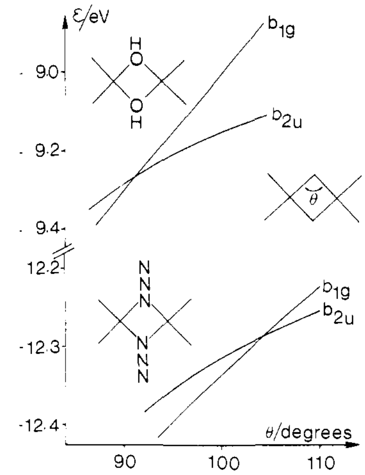

Figure 7. Variations of the energies of the b_{1g} and b_{2u} molecular orbitals vs. the bridging angle θ in planar bis(μ-hydroxo)copper(II) dimers and in planar bis(μ-azido)copper(II) dimers (see text).

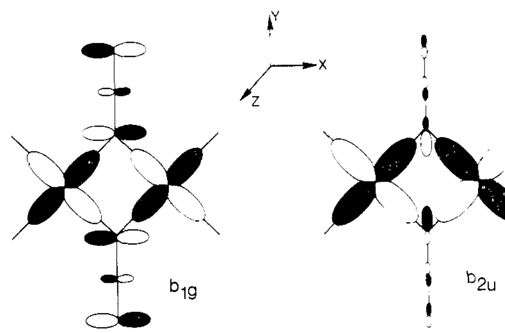

Figure 8. Schematic representation of b_{1g} and b_{2u} molecular orbitals in compound **1** (see text).

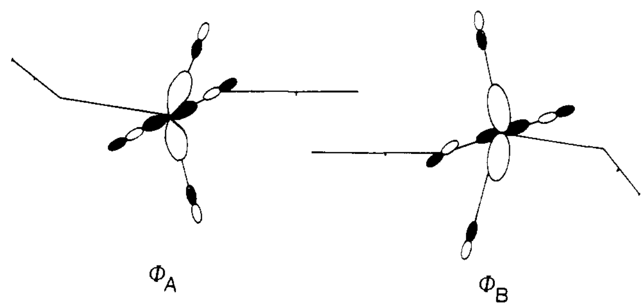

Figure 9. Schematic representation of the ϕ_A and ϕ_B magnetic orbitals in compound **2**.

Cu(II) ions of the same molecular entity. The spin densities described by ϕ_A and ϕ_B are essentially localized in parallel planes separated by 4.33 Å. The weak d_{z^2} contributions point in parallel directions and are centered on metallic ions too far away from each other to give a nonnegligible overlap, so the S and J_{AF} on the one hand and C and J_F on the other hand are zero.

In spite of the similarity of the cryptand cavities between **2** and **3**, their magnetic properties are drastically different. The disappearance of the antiferromagnetic coupling in **2** compared to **3** may be considered as a particularly spectacular example of *orbital reversal*.[45] The same phenomenon is observed when comparing the $[Cu_2(Me_5dien)_2(N_3)_2](BPh_4)_2$ complex[32] (dien = diethylenetriamine) to complex **3**.

Compound 3. The coordination skeleton relevant to the discussion of the magnetic properties of **3** is represented by **13**. All

(43) The calculation is of the extended Hückel type, with charge iteration on all the atoms and Madelung corrections. The choice of the atomic orbitals and of the parameters of the method was given in ref 39. The energies of the molecular orbitals were corrected from the shift due to the 2+ charge of the dimeric cations.

(44) Barraclough, C. G.; Brookes, R. W.; Martin, R. L. *Aust. J. Chem.* **1974**, *27*, 1843–1850.

(45) Girerd, J. J.; Verdaguer, M.; Kahn, O. *Inorg. Chem.* **1980**, *19*, 274–276. Verdaguer, M.; Michalowicz, A.; Girerd, J. J.; Alberding, N.; Kahn, O. *Inorg. Chem.* **1980**, *19*, 3271–3279.

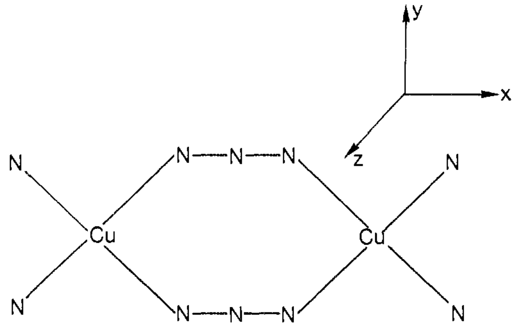

13

the atoms of this skeleton are coplanar. Again, we idealized somewhat the geometry by assuming a D_{2h} molecular symmetry. The d metal orbitals involved in the exchange phenomenon are the d_{xy}'s pointing toward the terminal and bridging nitrogen atoms. The highest occupied molecular orbitals for azide[46] are represented in Figure 10 (right). The essentially nonbonding π_g level is much higher in energy (−1.83 eV) than the $2\sigma_u$, $2\sigma_g$, and π_u levels immediately below (−8.51, −10.39, and −11.25 eV, respectively). It turns out that the energy difference between metallic d_{xy} orbitals and ligand orbitals is much weaker for the couple d_{xy}–π_g than for the couples d_{xy}–$2\sigma_u$, d_{xy}–$2\sigma_g$, or d_{xy}–π_u, so that the interaction d_{xy}–π_g is dominant. This interaction leads to molecular orbitals transforming as b_{1g} in the group D_{2h}. These molecular orbitals are antisymmetric with respect to the $\sigma(yz)$ mirror plane. The interaction d_{xy}–$2\sigma_u$ leads to molecular orbitals of the same b_{1g} symmetry. Thus, owing to the π_g–$2\sigma_u$ hybridization in the D_{2h} group, there will be three b_{1g} molecular orbitals, one very low in energy, the second weakly bonding or weakly antibonding, and the last one (ϕ_A) very high in energy. In the same way, the $2\sigma_g$ and π_u levels of the azido bridges are hydridized in the D_{2h} group to interact with d_{xy}, giving rise to three molecular orbitals transforming as b_{2u} and antisymmetric with respect to the $\sigma(yz)$ mirror plane; one is slightly stabilized compared to π_u, the second one is essentially nonbonding, and the third one (ϕ_S) is slightly destabilized with respect to d_{xy}. This correlation between metallic levels and ligand levels is schematized in Figure 10, where, for simplicity, the ligand levels not interacting with d_{xy} and the other d metallic orbitals are omitted. The energy gap Δ governing the magnitude of the antiferromagnetic coupling is defined by $\Delta = \epsilon(\phi_A) - \epsilon(\phi_S)$. In the present case, Δ is very large owing to the importance of the d_{xy}–π_g interaction between levels close in energy. Furthermore, we are in a situation where the molecular orbital description of the ground singlet state corresponding to the configuration $\phi_S{}^2\phi_A{}^0$ could be better than the Heitler–London description. Figure 11 represents the ϕ_S and ϕ_A molecular orbitals obtained from extended Hückel calculations, from which an energy gap $\Delta = 1.10$ eV is derived.[43]

Experimental Section

Materials and Analyses. The commercially available chemicals used were of reagent grade. Diethylenetriamine and 2-(2-chloroethoxy)-ethanol were purchased from Fluka A.G. and Aldrich Europe Co.

The ^{1}H NMR spectra were measured in $CDCl_3$ solution, with Me_4Si as internal reference, on a Varian A-60 or a XL-100 spectrometer at 60 or 100 MHz, respectively. The noise-decoupled ^{13}C NMR spectra were measured in $CDCl_3$ solution with Me_4Si as internal reference, on a Varian XL 100 or a Cameca 250 spectrometer at 25 or 62.86 MHz, respectively. Abbreviations are as follows: s, singlet: d. doublet; t, triplet; m, multiplet; br, broad.

The microanalyses were performed by the Service de Microanalyse of the CNRS. The mass spectra have been determined with a THN 208 spectrometer. The melting points have been measured on a Kofler block and are uncorrected. The purity of all compounds described have been checked by thin-layer chromatography on silica or on alumina.

Bis[2-(tosylamino)ethyl]tosylamine (7). A solution of diethylenetriamine (33.5 g,, 0.30 mol) in pyridine (70 mL) was added to 191 g (1.0 mol) of *p*-toluenesulfonyl chloride dissolved in 500 mL of pyridine at 50 °C. After reaction at 50 °C for 5 h with magnetic stirring, the mixture was cooled to room temperature, poured into 200 mL of water, and cooled in an ice bath with stirring. A white precipitate of the title compound was obtained; it was filtered, washed with ethanol, and dried; 158 g (85%); mp 175 °C (lit. mp 173–175 °C).[47]

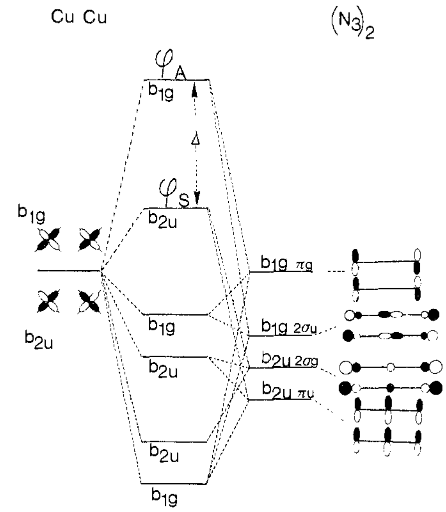

Figure 10. Correlation between metallic levels and ligand levels for complex **3** (see text).

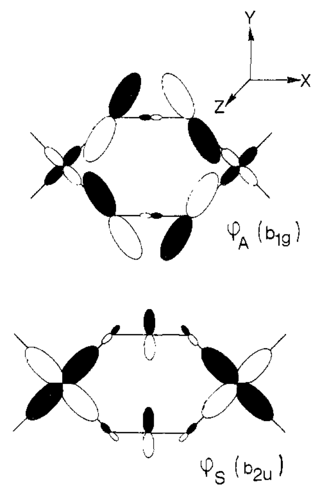

Figure 11. Schematic representation of ϕ_S and ϕ_A molecular orbitals in compound **3** as obtained by extended Hückel calculations (see text).

6,9,12-Triaza-3,15-dioxa-6,9,12-tritosylheptadecane-1,17-diol (8). A mixture of diethylenetriamine tritosylate **7** (84.75 g, 0.15 mol), 2-(2-chloroethoxy)ethanol (commercial, 150 g), and potassium carbonate (82.8 g) were heated in a 500-mL round-bottomed flask at 100 °C for 72 h with efficient stirring. After cooling to room temperature, the mixture was filtered and the solid residue washed on the filter with 100 mL of methylene chloride. The methylene chloride was removed from the combined filtrate at the rotatory evaporator and the excess of 2-(2-chloroethoxy)ethanol distilled under reduced pressure (60 °C (1.2 mmHg)). The oily residue was taken up in 100 mL of methylene chloride and chromatographed on silica with methylene chloride as eluant. After evaporation of the solvent, pure diol **8** was obtained as a colorless oil: 100 g (90%); ^{1}H NMR δ 2.43 (s, 9 H, 3 CH_3), 3.25–3.82 (brm, 24 H, 6 NCH_2, 6 OCH_2). 7.26, 7.38, 7.68, 7.82 (2 d, 12 H, Ar H); ^{13}C NMR δ 21.3 (CH_3), 49.0, 49.2, 49.6 (CH_2N), 61.4 (CH_2OH). 69.9, 72.5 (CH_2O), 172.2, 129.8, 135.3, 135.8, 143.5, 143.8 (Ar C). Anal. Calcd for $C_{33}H_{47}N_3O_{10}S_3$ (741.9): C, 53.42; H, 6.39. Found: C, 53.10; H, 6.08.

6,9,12-Triaza-3,15-dioxa-6,9,12-tritosyl-1,17-bis(tosyloxy)heptadecane (9). Diol **8** (105 g, 141 mmol) dissolved in pyridine (250 mL) was added over 5 h with efficient stirring to a solution of *p*-toluenesulfonyl chloride

(46) Wyatt, J. F.; Hillier, I. H.; Saunders. V. R.: Connor, J. A.: Barber, M. *J. Chem. Phys.* **1971**, *54*, 5311–5315.

(47) Atkins, T. J.; Richman, J. E.; Oettle. W. F. *Org. Synth.* **1978**, *58*, 86–98.

(48) Supplementary material.

Table IV. Crystal Data and Data Collection Details for $1\cdot H_2O$ and for 2

formula	$Cu_2^{II}(N_3)_4(C_{16}H_{34}N_2O_6)(H_2O)$, $1\cdot H_2O$ $Cu_2(N_3)_4$([24]ane-1,13-N_2-4,7,10,16,19,22-O_6)(H_2O) $Cu_2C_{16}H_{36}N_{14}O_7$	$[Cu^{II}(N_3)_2]_2(C_{16}H_{38}N_6O_2)$, 2 $[Cu(N_3)_2]_2$([24]ane-1,4,10,13,16,22-N_4-7,19-O_2) $Cu_2C_{16}H_{38}N_{18}O_2$
R_F, R_{wF}	0.034, 0.048	0.040, 0.060
M_r	645.62	641.68
space group	$P21/n$ (alternate setting of $P21/c$)	C_{2h}^3-$C2/m$ (no. 12)
a, Å	17.780 (2)	9.533 (1)
b, Å	9.719 (1)	12.305 (1)
c, Å	17.361 (2)	11.913 (1)
β, deg	109.32 (5)	107.25 (4)
V, Å^3	2831.0	1334.0
Z, formula units	4	2
$\rho_{calcd}(\rho_{obsd})$, g cm^{-3}	1.515 (1.5)	1.597 (1.6)
data coll temp, K	291	293
radiation, Å	graphite monochromated Cu $\lambda_{K^-\alpha} = 1.541\ 84$	graphite monochromated Cu $\lambda_{K^-\alpha} = 1.541\ 84$
linear coeff abs, cm^{-1}	23.9	24.6
scan speed	0.02° in 2θ/s	2.0° in 2θ/min
standard	1000, 060, 0010; 48 measmt each	600, 080, 55$\bar{6}$; 48 measmt each
λ^{-1} sin θ limits, Å^{-1}	0.0298–0.5396	0.0439–0.6089
2θ limits, deg	5.26–112.60	7.76–139.71
fudge factor p	0.05	0.07
unique data	4133	1394
unique data with $F_o^2 > 3\sigma(F_o^2)$	3376	1216

(54 g, 282 mmol) in pyridine (200 mL) cooled in an ice bath. The reaction mixture was kept overnight in a refrigerator at 4 °C and then poured over 600 g of ice, with stirring until the ice melted. The very viscous oil obtained was separated from the water–pyridine mixture by pouring over a filter paper in a Büchner funnel without suction and then dissolving in 500 mL of methylene chloride. The organic phase was washed three times with 200 mL of 1 N HCl and twice with 200 mL of a saturated NaCl solution, and then dried over Na_2SO_4, and evaporated to dryness. The crude product was chromatographed on silica with methylene chloride as eluant, giving the desired compound **9** as a colorless oil: 110 g (74%); ^{1}H NMR δ 2.43 (s, 15 H, 5 CH_3), 3.12–3.82 (brm, 20 H, 6 NCH_2, 5 OCH_2), 4.12 (brt, 4 H, CH_2OTs), 7.26, 7.38, 7.68, 7.82 (2 d, 20 H, Ar H); ^{13}C NMR δ 21.4 (CH_3), 48.8, 49.1 (CH_2N), 68.3, 69.0, 69.8 (CH_2O), 127.2, 127.8, 129.9, 132.9, 135.6, 135.9, 143.6, 143.7, 144.9 (Ar C). Anal. Calcd for $C_{47}H_{59}O_{14}S_5$ (105.3): C, 53.74; H, 5.66; N, 4.00. Found: C, 52.68; H, 5.50; N, 4.45.

1,13-Dioxa-4,7,10,16,19,22-hexaaza-4,7,10,16,19,22-hexatosylcyclotetracosane (6b). Tritosyl diethylene triamine **7** (5.65 g, 10 mmol) was added to a solution of sodium (0.46 g, 20 mmol) in anhydrous methanol (100 mL). After 2 h at reflux, the solvent was evaporated under vacuum and the residue dried under low pressure (0.1 mmHg). The disodium salt thus obtained was dissolved in 100 mL of anhydrous DMF and heated to 80 °C. To this solution, 10.5 g (10 mmol) of **9** dissolved in 120 mL of anhydrous DMF was added over 90 min with stirring. After 1 h, 100 mL of water was added dropwise; the mixture was cooled to room temperature and left overnight with stirring. The white precipitate was filtered, washed with ethanol, dried, and crystallized from methylene chloride. The product thus obtained was a mixture of the desired 24-membered macrocycle **6b** and of the (1 + 1) condensation product, 1,4,7-triaza-10-oxa-1,4,7-tritosylcyclododecane (10.2 g (80%)). A small quantity of the crude material was purified at this stage for analytical purposes by several recrystallizations from methylene chloride until thin-layer chromatography and NMR spectroscopy indicated that the product was pure. From the amount obtained, the crude material was calculated to contain more than 80% of the desired compound 6b: mp 202 °C; ^{1}H NMR δ 2.4 (s, 18 H, CH_3), 3.35, 3.50 (s + m, 32 H, NCH_2, OCH_2), 7.25, 7.65 (q, 24 H, Ar H); ^{13}C NMR δ 21.4 (CH_3), 47.5, 50.5 (CH_2N), 71.8 (CH_2O), 127.3, 129.8, 135.1, 137.0, 143.3, 143.6 (Ar C). Anal. Calcd for $C_{58}H_{74}N_6O_{14}S_6$ (M_r 1270): C, 54.80; H, 5.82; N, 6.61. Found: C, 54.81; H, 5.94; N, 6.71.

1,13-Dioxa-4,7,10,16,19,23-hexaazacyclotetracosane (5). A solution of 33% HBr in acetic acid (350 mL) was added to a mixture of 32.5 g of the crude product obtained above and phenol (47 g, 0.5 mol). After being heated at 80 °C for 48 h with efficient stirring, the mixture was cooled to room temperature and the solvent evaporated under vacuum. The remaining acetic acid was eliminated by twice adding 200 mL of toluene and evaporating. The brown oily residue was dissolved in 500 mL of water and the solution extracted six times with 100 mL of methylene chloride. The aqueous phase was evaporated, and the orange oil obtained was redissolved in 20 mL of water and passed over a quaternary ammonium anion exchange column in the hydroxide form (Dowex 1). The aqueous solution obtained was evaporated, leaving a yellow oily residue (10.2 g), which contained a mixture of **5** and of 1,4,7-triaza-10-oxacyclododecane. The latter was removed by sublimation at 80 °C under low pressure (0.01 mmHg). The residual compound **5** was transformed into its hexahydrochloride by dissolving in 30 mL of 1 N HCl and evaporating. This salt was purified by crystallization from an ethanol–water mixture (95/5). The free hexaamine was regenerated by passing the hexahydrochloride over an anion exchange column in the hydroxide form (Dowex 1 × 8). After evaporation of the aqueous solution, the pure macrocyclic hexaamine **5** was obtained as a colorless oil, which crystallizes on standing in the cold at −35 °C; 2.0 g (90%); ^{1}H NMR δ 1.8 (s, 6 H, NH), 2.75 (s + t, 24 H, NCH_2), 3.60 (t, 8 H, OCH_2); ^{13}C NMR (D_2O; reference, CH_3 of *tert*-butyl alcohol) δ 47.8, 49.1 (CH_2N), 70.6 (CH_2O). Anal. Calcd for $C_{16}H_{38}N_6O_2\cdot 6HCl\cdot 4H_2O$ (M_r 637.3): C, 30.11; H, 8.16; N, 13.15. Found: C, 29.92; H, 8.25; N, 13.19.

Preparation of the Bis Copper(II) Complex 1 of the Macrocycle 4. All preparations of copper(II) complexes have been conducted by using only glass flasks and instruments in order to avoid contamination by ferromagnetic impurities. A solution of 125 mg Cu $(ClO_4)_2\cdot 6H_2O$ mL of methanol was added to a solution of 50 mg of the [24]ane-N_2O_6 macrocycle **4** obtained in previous work.[21] The solution was evaporated and the solid obtained filtered and washed with 20 mL of cold methanol. It was then dissolved in 20 mL of water, and 40 mg of sodium azide was added. On standing at room temperature, green crystals of the bis $Cu(N_3)_2$ complex **1** are obtained as $1\cdot H_2O$. These crystals were used for the crystal structure determination and for the magnetic measurements. The compound was dried under vacuum for microanalysis. Anal. Calcd for $C_{16}H_{34}N_2O_6\cdot 2Cu(N_3)_2$ (M_r 645.6): C, 29.76; H, 5.30; N, 30.37. Found: C, 29.71; H, 5.17; N, 30.20.

Preparation of the Bis Copper(II) Complex 2 of the Macrocycle 5. A solution of 100 mg of $Cu(ClO_4)_2\cdot 6H_2O$ in 20 mL of ethanol was added to a solution of 40 mg of **5** in 20 mL of methanol. The intensely blue solution obtained was evaporated to half of its volume. A blue precipitate of the bis $Cu(ClO_4)_2$ complex of **5** was obtained. Anal. Calcd for $C_{16}H_{38}N_6O_2\cdot 2Cu(ClO_4)_2\cdot 4H_2O$ (M_r 943.5): C, 20.36; H, 4.91; N, 8.91. Found: C, 19.22; H, 4.52; N, 9.22.

A solution of 30 mg of sodium azide in 10 mL of water was added to a solution of 60 mg of the previous complex in 20 mL of water. The color of the solution changed from blue to green. On standing the bis $Cu(N_3)_2$ complex **2** of **5** crystallized slowly. These crystals were used for the crystal structure determination and for the magnetic measurements. Anal. Calcd for $C_{16}H_{38}N_6O_2\cdot 2Cu(N_3)_2$ (M_r 641.7): C, 29.95; H, 5.97; N, 39.29. Found: C, 29.80; H, 5.83; N, 39.40.

Crystal Structure Determinations

X-ray Structure of the Copper(II) Complex of [24]ane-N_2O_6 (1). Crystals of $1\cdot H_2O$, $Cu^{II}_2(N_3)_4(C_{16}H_{34}N_2O_6)(H_2O)$, were grown by slow evaporation of an aqueous solution of the product. A systematic search in reciprocal space using a Philips PW 1100 automatic diffractometer showed that crystals of **1** belong to the monoclinic system and that the space group is $P2_1/n$, alternative setting of $P2_1/c$. Precise lattice parameters and their estimated standard deviations were determined by using 25 hand-selected high-2θ angle accurately centered reflections (λ^{-1} sin $\theta > 0.35$ Å^{-1} with use of $\lambda_{K\alpha_1\ Cu}$ radiation). Crystal data and im-

Table V. Positional and Thermal Parameters and Their Estimated Standard Deviations for $Cu^{II}_2(N_3)_4(C_{16}H_{34}N_2O_6)(H_2O)(1\cdot H_2O)$. The Form of the Anisotropic Thermal Parameter is $\exp[-(\beta_{11}h^2 + \beta_{22}k^2 + \beta_{33}l^2 + \beta_{12}hk + \beta_{13}hl + \beta_{23}kl)]$

atom	x	y	z	β_{11}	β_{22}	β_{33}	β_{12}	β_{13}	β_{23}
Cu1	0.42617 (2)	0.43014 (5)	0.26989 (3)	0.00247 (1)	0.00716 (5)	0.00283 (2)	0.00120 (4)	0.00240 (2)	−0.00110 (5)
Cu2	0.55891 (2)	0.61636 (4)	0.23845 (2)	0.00198 (1)	0.00699 (5)	0.00282 (2)	−0.00041 (4)	0.00222 (2)	−0.00159 (5)
O4	0.4878 (1)	0.3474 (3)	0.4206 (1)	0.00420 (9)	0.0107 (3)	0.00347 (9)	0.0010 (3)	0.0027 (1)	0.0012 (3)
O7	0.6493 (2)	0.3156 (3)	0.4364 (1)	0.00556 (10)	0.0143 (4)	0.00338 (10)	0.0033 (3)	0.0025 (1)	−0.0007 (3)
O10	0.6787 (1)	0.5796 (3)	0.3813 (1)	0.00291 (8)	0.0112 (3)	0.00354 (10)	0.0020 (3)	−0.0001 (1)	0.0000 (3)
O16	0.4847 (1)	0.7821 (2)	0.1240 (1)	0.00302 (7)	0.0094 (3)	0.00252 (8)	−0.0010 (2)	0.0016 (1)	0.0001 (2)
O19	0.3571 (1)	0.6044 (2)	0.0421 (1)	0.00330 (8)	0.0096 (3)	0.00336 (3)	0.0000 (2)	0.0020 (1)	−0.0010 (3)
O22	0.2958 (1)	0.5021 (2)	0.1543 (1)	0.00238 (7)	0.0124 (3)	0.00305 (9)	−0.0012 (2)	0.0010 (1)	−0.0003 (3)
O0	0.3031 (1)	0.8135 (3)	0.1415 (2)	5.23 (6)					
N25	0.5094 (1)	0.4314 (2)	0.2164 (2)	0.00305 (9)	0.0074 (3)	0.00376 (10)	0.0002 (3)	0.0032 (1)	−0.0021 (3)
N26	0.5352 (1)	0.3354 (3)	0.1878 (1)	0.00364 (9)	0.0076 (3)	0.00268 (9)	−0.0010 (3)	0.0031 (1)	0.0003 (3)
N27	0.5602 (2)	0.2477 (3)	0.1610 (2)	0.00687 (12)	0.0084 (3)	0.00560 (11)	0.0010 (3)	0.0080 (2)	−0.0024 (3)
N28	0.4724 (1)	0.6244 (3)	0.2911 (2)	0.00260 (8)	0.0076 (3)	0.00410 (10)	−0.0005 (3)	0.0040 (1)	−0.0019 (3)
N29	0.4523 (1)	0.7248 (3)	0.3203 (1)	0.00233 (7)	0.0096 (3)	0.00315 (9)	−0.0004 (3)	0.0026 (1)	0.0005 (3)
N30	0.4343 (2)	0.0204 (3)	0.3400 (2)	0.00452 (10)	0.0105 (4)	0.00572 (12)	0.0010 (3)	0.0058 (2)	−0.0020 (4)
N31	0.3972 (2)	0.2356 (3)	0.2478 (2)	0.00528 (11)	0.0088 (3)	0.00392 (11)	−0.0037 (3)	0.0039 (2)	−0.0016 (3)
N32	0.3036 (1)	0.1789 (3)	0.1841 (2)	0.00303 (9)	0.0090 (3)	0.00506 (12)	−0.0015 (3)	0.0036 (1)	−0.0017 (3)
N33	0.3687 (2)	0.1181 (4)	0.1239 (2)	0.00569 (14)	0.0179 (5)	0.00563 (14)	−0.0049 (4)	0.0049 (2)	−0.0098 (4)
N34	0.6298 (1)	0.5858 (3)	0.1737 (2)	0.00299 (9)	0.0139 (4)	0.00376 (11)	0.0014 (3)	0.0035 (1)	−0.0017 (3)
N35	0.6928 (1)	0.5339 (3)	0.2007 (2)	0.00359 (9)	0.0146 (4)	0.00404 (11)	0.0029 (3)	0.0041 (1)	−0.0016 (4)
N36	0.7538 (2)	0.4834 (6)	0.2227 (2)	0.00565 (13)	0.0427 (9)	0.00794 (20)	0.0194 (5)	0.0064 (2)	0.0828 (7)
N1	0.3409 (1)	0.4541 (3)	0.3231 (2)	0.00255 (8)	0.0094 (3)	0.00308 (29)	−0.0013 (3)	0.0026 (1)	−0.0003 (3)
N13	0.6091 (1)	0.8014 (3)	0.2754 (1)	0.00218 (7)	0.0084 (3)	0.00266 (9)	−0.0012 (3)	0.0017 (1)	−0.0016 (3)
C2	0.3736 (2)	0.4792 (4)	0.4118 (2)	0.0037 (1)	0.0127 (5)	0.0031 (1)	−0.0024 (4)	0.0037 (2)	−0.0024 (4)
C3	0.4249 (2)	0.3610 (4)	0.4535 (2)	0.0047 (1)	0.0146 (5)	0.0028 (1)	−0.0036 (5)	0.0026 (2)	0.0009 (4)
C5	0.5290 (3)	0.2191 (4)	0.4408 (2)	0.0063 (2)	0.0104 (5)	0.0032 (2)	0.0004 (5)	0.0010 (3)	0.0008 (5)
C6	0.5920 (2)	0.2148 (4)	0.4022 (3)	0.0063 (2)	0.0106 (4)	0.0040 (2)	0.0059 (5)	0.0018 (3)	0.0000 (5)
C8	0.7027 (2)	0.3408 (4)	0.3927 (2)	0.0062 (2)	0.0144 (5)	0.0049 (2)	0.0097 (5)	0.0044 (2)	0.0030 (5)
C9	0.7390 (2)	0.4779 (5)	0.4144 (2)	0.0037 (1)	0.0173 (6)	0.0042 (2)	0.0064 (5)	0.0021 (2)	0.0033 (5)
C11	0.7099 (2)	0.7141 (4)	0.4003 (2)	0.0031 (1)	0.0146 (5)	0.0036 (2)	−0.0020 (5)	0.0001 (2)	−0.0020 (5)
C12	0.6438 (2)	0.8155 (4)	0.3648 (2)	0.0031 (1)	0.0095 (4)	0.0036 (1)	−0.0024 (4)	0.0019 (2)	−0.0033 (4)
C14	0.5573 (2)	0.9187 (4)	0.2357 (2)	0.0033 (1)	0.0074 (4)	0.0037 (1)	−0.0019 (3)	0.0026 (2)	−0.0010 (4)
C15	0.5299 (2)	0.9046 (3)	0.1457 (2)	0.0033 (1)	0.0007 (4)	0.0038 (1)	−0.0018 (3)	0.0027 (2)	0.0008 (4)
C17	0.4603 (2)	0.7571 (4)	0.0382 (2)	0.0039 (1)	0.0146 (5)	0.0025 (1)	−0.0017 (4)	0.0022 (2)	0.0006 (4)
C18	0.4271 (2)	0.6139 (4)	0.0212 (2)	0.0039 (1)	0.0140 (5)	0.0026 (1)	0.0001 (4)	0.0023 (2)	−0.0032 (4)
C20	0.3276 (2)	0.4687 (4)	0.0352 (2)	0.0049 (2)	0.0110 (4)	0.0020 (1)	−0.0021 (5)	0.0000 (2)	−0.0023 (4)
C21	0.2631 (2)	0.4635 (4)	0.0718 (2)	0.0035 (1)	0.0120 (5)	0.0039 (2)	−0.0028 (4)	0.0002 (2)	−0.0004 (5)
C23	0.2384 (2)	0.5105 (4)	0.1950 (2)	0.0021 (1)	0.0134 (5)	0.0052 (2)	0.0002 (4)	0.0020 (2)	0.0036 (5)
C24	0.2798 (2)	0.5549 (4)	0.2805 (2)	0.0025 (1)	0.0126 (4)	0.0043 (1)	0.0006 (4)	0.0034 (2)	0.0015 (4)

Table VI. Positional and Thermal Parameters and Their Estimated Standard Deviations for $[(Cu^{II}(N_3)_2]_2(C_{16}H_{38}N_6O_2)$ (2). The Form of the Anisotropic Thermal Parameter is $\exp[-(\beta_{11}h^2 + \beta_{22}k^2 + \beta_{33}l^2 + \beta_{12}hk + \beta_{13}hl + \beta_{23}kl)]$

atom	x	y	z	β_{11}	β_{22}	β_{33}	β_{12}	β_{13}	β_{23}
Cu	−0.02680 (7)	0.0000 (0)	0.25651 (5)	0.00753 (6)	0.00461 (4)	0.00263 (3)	0.0000 (0)	0.00264 (7)	0.0000 (0)
O7	0.0000 (0)	−0.2557 (3)	0.5000 (0)	0.0150 (4)	0.0039 (2)	0.0040 (2)	0.0000 (0)	0.0057 (4)	0.0000 (0)
N1	−0.1573 (4)	0.0000 (0)	0.1173 (3)	0.0077 (4)	0.0050 (2)	0.0027 (2)	0.0000 (0)	0.0030 (4)	0.0000 (0)
N4	−0.0334 (3)	−0.1599 (2)	0.2757 (2)	0.0081 (2)	0.0042 (2)	0.0036 (1)	0.0026 (3)	0.0048 (3)	0.0002 (3)
N25	0.1917 (4)	0.0000 (0)	0.4018 (3)	0.0076 (4)	0.0076 (3)	0.0031 (2)	0.0000 (0)	0.0023 (5)	0.0000 (0)
N26	0.1792 (4)	0.0000 (0)	0.4980 (3)	0.0055 (3)	0.0050 (2)	0.0043 (2)	0.0000 (0)	0.0017 (4)	0.0000 (0)
N27	0.1780 (5)	0.0000 (0)	0.5950 (3)	0.0102 (4)	0.0078 (3)	0.0037 (2)	0.0000 (0)	0.0049 (5)	0.0000 (0)
N28	0.1618 (0)	0.0000 (0)	0.1373 (0)	0.0082 (0)	0.0155 (0)	0.0037 (0)	0.0000 (0)	0.0066 (0)	0.0000 (0)
N29	0.2915 (4)	0.0000 (0)	0.1617 (3)	0.0107 (4)	0.0061 (3)	0.0027 (2)	0.0000 (0)	0.0046 (4)	0.0000 (0)
N30	0.4176 (5)	0.0000 (0)	0.1808 (4)	0.0093 (5)	0.0090 (4)	0.0070 (3)	0.0000 (0)	0.0042 (7)	0.0000 (0)
C2	−0.2423 (3)	−0.1005 (3)	0.1165 (3)	0.0089 (3)	0.0054 (2)	0.0048 (2)	−0.0021 (5)	0.0025 (4)	0.0001 (4)
C3	−0.1366 (4)	−0.1927 (3)	0.1611 (3)	0.0115 (4)	0.0049 (2)	0.0044 (2)	−0.0003 (5)	0.0047 (4)	−0.0014 (4)
C5	0.0767 (3)	−0.2448 (3)	0.3301 (3)	0.0092 (3)	0.0051 (2)	0.0057 (2)	0.0046 (4)	0.0058 (4)	0.0006 (4)
C6	0.0255 (4)	−0.3199 (3)	0.4088 (3)	0.0110 (4)	0.0044 (2)	0.0050 (2)	0.0029 (5)	0.0033 (5)	−0.0006 (4)

portant details and data collection are summarized in Table IV.

Solution and Refinement of the Structure of 1. Diffraction data were collected at 293 K with use of Cu Kα radiation from a highly oriented monochrometer by using the $\theta/2\theta$ scan technique. The intensities of three standard reflections were measured every 2 h during the entire data collection period and showed no variation. Only those 3376 reflections having $F_o^2 > 3\sigma(F_o^2)$ were used in the structure calculation. The usual procedures, computer programs, atomic scattering factors, and anomalous dispersion terms were used in the solution and refinement of the structure (Enraf-Nonius SDP/V17 with digital PDP 11/60 computer). Coordinates for the copper atoms were obtained from a three-dimensional Patterson synthesis. All other atoms appeared in subsequent Fourier synthesis. Most of the hydrogen atoms were located in difference Fourier syntheses, and all were included as a fixed contribution to F_c at their idealized positions (C–H = 0.95 Å, C–C–H = 109.5°, B(H) = 5.0 Å^2). The final three cycles of refinement, where all atoms except the hydrogen atoms were assigned anisotropic thermal parameters, converged to the values for R and R_w on F^2 of 0.034 and 0.048, respectively, for the 347 variables and 2842 data. The standard error in an observation of unit weight is 2.0 e^2. The highest peak in the final difference Fourier map had height <0.15 e Å^{-3}.

Final parameters xyz, β_{ij} are given in Table V for all non-hydrogen atoms. Table VI[30] lists the values of hkl, $10|F_o|$ vs. $10|F_c|$.

X-ray Structure of the Copper(II) Complex of [24]ane-N$_6$O$_2$ (2). Solution and Refinement. Crystals of **2** ($Cu^{II}(N_3)_2)_2(C_{16}H_{38}N_6O_2)$) suitable for X-ray study were selected after recrystallization of the product by slow evaporation of an aqueous solution at room temperature. A systematic search in reciprocal space using an Enraf-Nonius four-circle CAD-4 automatic diffractometer controlled by a PDP 8a computer showed that crystals of **2** belong to the monoclinic system and that the space group is $C2$, Cm, or $C2/m$. The lattice parameters and the data collection were obtained as described for compound **1**. Crystal data and details of the data collection are summarized in Table IV. The resolution of this structure was carried out in the same way as was done for **1**. The final least-squares cycle converged to values of R and R_w on F^2 of 0.040 and 0.060, respectively, for the 99 variables and 1216 data. The standard error in an observation of unit weight is 1.37 e^2. The highest density in the final difference Fourier map is <0.10 e $Å^{-3}$. Final xyz, β_{ij} non-hydrogen parameters are listed in Table VI. Table VIII[30] lists the values of hkl, $10|F_o|$ vs. $10|F_c|$.

Magnetic Measurements

The magnetic susceptibility measurements were carried out with a Faraday-type magnetometer equipped with a continuous-flow cryostat in the temperature range 3.8–300 K. The polycrystalline powder samples weighed about 7 mg. The applied magnetic fields were in the range 0.3–0.6 T. The independence of the susceptibility against the magnetic field was checked at both room temperature and 20 K. Mercury tetrakis(thiocyanato)cobaltate(II) was used as a susceptibility standard. The uncertainty on the temperature T is estimated as 0.1 K. The uncertainty on the molar magnetic susceptibility χ_M is more difficult to appreciate. If the uncertainty on the measurement itself is less than 2% as shown by the reproductibility of the magnetic curves carried out on different samples of the same compound, the uncertainty on the temperature-independent susceptibility, including diamagnetism and TIP, is probably rather high. The magnetic data were corrected for that, and these corrections were estimated as -290×10^{-6} cm^3 mol^{-1} for **1** and -250×10^{-6} cm^3 mol^{-1} for **2**. If an uncertainty of 50×10^{-6} cm^3 is assumed for these values, the uncertainty on $\chi_M T$ is as large as 0.03 cm^3 mol^{-1} K. It will be important to keep in mind this $\Delta\chi_M T$ value when interpreting the magnetic data.

EPR Measurements

The EPR study was carried out on a crystal of **1**·H_2O and on a powder sample of **2** in the 4.2–300 K temperature range with a Bruker ER 200 spectrometer equipped with a continuous-flow cryostat and working in the X-band. A 100-KHz field modulation was used, and the magnetic fields were measured by a Hall probe.

Registry No. **1**·H_2O, 83095-47-0; **2**, 83095-48-1; **3**, 71072-85-0; **5**, 43090-52-4; **6b**, 83076-80-6; **7**, 56187-04-3; **8**, 83076-78-2; **9**, 83076-79-3; 2-(2-chloroethoxy)ethanol, 628-89-7; *p*-toluenesulfonyl chloride, 98-59-9.

Supplementary Material Available: Tables VII and VIII, listing the values of hkl, $10|F_o|$ vs. $10|F_c|$ for **1**·H_2O and **2**, respectively; Figures 12 and 13, showing the packing in the unit cell for **1** and **2**, respectively (21 pages). Ordering information is given on any current masthead page.

Photochemical Reaction of Dirhenium Decacarbonyl with Water[1]

David R. Gard and Theodore L. Brown*

Contribution from The School of Chemical Sciences, University of Illinois, Urbana, Illinois 61801. *Received February 11, 1982*

Abstract: The photochemical reaction of $Re_2(CO)_{10}$ with H_2O in THF and other solvents has been studied, with use of radiation of varying wavelength. The initial reaction leads to $Re_2(CO)_9(OH_2)$, formed upon irradiation at 313 nm. This product is shown to form via a primary photochemical homolysis of the Re–Re bond, followed by thermal substitution of the $Re(CO)_5\cdot$ radical by H_2O, and then re-formation of the metal–metal bond to give $Re_2(CO)_9(OH_2)$. Although $Re_2(CO)_9(OH_2)$ is relatively stable toward 313-nm irradiation, it decomposes rapidly under 366-nm irradiation to form $HRe(CO)_5$ and $Re_4(CO)_{12}(OH)_4$. The decomposition pathway is thought to involve $Re_2(CO)_8(OH_2)_2$, an unstable intermediate. The presence of this intermediate is substantiated in part by the observation that thermal reaction of $Re_2(CO)_8(CH_3CN)_2$ with H_2O in THF leads to formation of $Re_4(CO)_{12}(OH)_4$. The decomposition of $Re_2(CO)_8(OH_2)_2$ is proposed to proceed via initial loss of H_2O and oxidative addition of an O–H bond to form (μ-hydrido)(μ-hydroxo)dirhenium octacarbonyl, $HRe_2(CO)_8(OH)$, which undergoes decomposition to form the observed products.

Introduction

Herberhold and Süss have reported[2,3] that photolysis of $Re_2(CO)_{10}$ in wet ether solution results in quantitative conversion to the tetranuclear hydroxo compound $Re_4(CO)_{12}(OH)_4$, with evolution of H_2 (eq 1). The only intermediate observed during the

$$2Re_2(CO)_{10} + 4H_2O \rightarrow Re_4(CO)_{12}(OH)_4 + 2H_2 + 8CO \quad (1)$$

reaction was $H_3Re_3(CO)_{12}$. This reaction, which results in partial water splitting, is of synthetic and mechanistic interest, particularly since few stable transition-metal hydroxocarbonyl compounds are known. The pathway leading to formation of the product is not evident, and the failure to observe several rhenium carbonyl compounds that might be expected as intermediates is not readily accounted for. Accordingly, we have reinvestigated this reaction in some detail, paying attention to the dependence of the reaction on irradiation wavelength. Our results show that the reaction follows an unexpected route; the use of varying wavelengths of irradiation has made it possible to isolate intermediates along the pathway to the final product.

Experimental Section

Reagents. Dirhenium decacarbonyl, $Re_2(CO)_{10}$, and triosmium dodecacarbonyl, $Os_3(CO)_{12}$, were purchased from Pressure Chemical Co. and Strem Chemical Co., respectively, and used without further purification.

Deionized water was purified by passing through a mixed bed of IR-20 and A-101D ion-exchange resins (Dearborn Chemical). The water was degassed prior to use by boiling.

Linde CP carbon monoxide, CO, was passed through activated manganese(II) oxide and 3A molecular sieves to reduce levels of O_2 and H_2O, respectively.

Trimethylamine *N*-oxide dihydrate, $Me_3NO\cdot 2H_2O$, was obtained from Aldrich Chemical Co. (98%) and used without further purification.

Hydridorhenium pentacarbonyl, $HRe(CO)_5$, was prepared by acidification of $NaRe(CO)_5$.[4]

(1) This research was supported by the National Science Foundation through Research Grants CHE76-17570 and CHE79-13-8010730.

(2) Herberhold, M.; Süss, G. *Angew. Chem., Int. Ed. Engl.* **1975**, *14*, 700.

(3) Herberhold, M.; Süss, G.; Ellermann, J.; Gabelein, H. *Chem. Ber.* **1978**, *111*, 2931.

(4) Byers, B. H. Ph.D. Thesis, University of Illinois, Urbana-Champaign, IL, 1975.

